Journal of Biomedical Optics

BiomedicalOptics.SPIEDigitalLibrary.org

Enhancing *in vivo* tumor boundary delineation with structured illumination fluorescence molecular imaging and spatial gradient mapping

Jessica Sun
Jessica P. Miller
Deep Hathi
Haiying Zhou
Samuel Achilefu
Monica Shokeen
Walter J. Akers

SPIE.

Jessica Sun, Jessica P. Miller, Deep Hathi, Haiying Zhou, Samuel Achilefu, Monica Shokeen, Walter J. Akers, "Enhancing *in vivo* tumor boundary delineation with structured illumination fluorescence molecular imaging and spatial gradient mapping," *J. Biomed. Opt.* **21**(8), 080502 (2016), doi: 10.1117/1.JBO.21.8.080502.

Enhancing *in vivo* tumor boundary delineation with structured illumination fluorescence molecular imaging and spatial gradient mapping

Jessica Sun,[a,†] Jessica P. Miller,[a,b,†] Deep Hathi,[a,b] Haiying Zhou,[a] Samuel Achilefu,[a,b,c] Monica Shokeen,[a] and Walter J. Akers[a,*]

[a]Washington University School of Medicine, Department of Radiology, 4515 McKinley Avenue, St. Louis, Missouri 63110, United States

[b]Washington University School of Medicine, Department of Biomedical Engineering, 4515 McKinley Avenue, St. Louis, Missouri 63110, United States

[c]Washington University School of Medicine, Department of Biochemistry and Molecular Biophysics, 4515 McKinley Avenue, St. Louis, Missouri 63110, United States

Abstract. Fluorescence imaging, in combination with tumor-avid near-infrared (NIR) fluorescent molecular probes, provides high specificity and sensitivity for cancer detection in preclinical animal models, and more recently, assistance during oncologic surgery. However, conventional camera-based fluorescence imaging techniques are heavily surface-weighted such that surface reflection from skin or other nontumor tissue and nonspecific fluorescence signals dominate, obscuring true cancer-specific signals and blurring tumor boundaries. To address this challenge, we applied structured illumination fluorescence molecular imaging (SIFMI) in live animals for automated subtraction of nonspecific surface signals to better delineate accumulation of an NIR fluorescent probe targeting $\alpha_4\beta_1$ integrin in mice bearing subcutaneous plasma cell xenografts. SIFMI demonstrated a fivefold improvement in tumor-to-background contrast when compared with other full-field fluorescence imaging methods and required significantly reduced scanning time compared with diffuse optical spectroscopy imaging. Furthermore, the spatial gradient mapping enhanced highlighting of tumor boundaries. Through the relatively simple hardware and software modifications described, SIFMI can be integrated with clinical fluorescence imaging systems, enhancing intraoperative tumor boundary delineation from the uninvolved tissue.
[DOI: 10.1117/1.JBO.21.8.080502]

Keywords: biomedical imaging; preclinical; optical; molecular imaging; cancer; spatial frequency domain; cancer; surgery.

Paper 160453LRR received Jul. 5, 2016; accepted for publication Aug. 5, 2016; published online Aug. 31, 2016.

*Address all correspondence to: Walter J. Akers, E-mail: akersw@mir.wustl.edu

†Co-contributing first authors

Surgical resection of cancer is the primary treatment for accessible areas including breast and head and neck regions. Cancer is difficult to distinguish from adjacent nontumor tissues, resulting in inadequate margins of resection and a high rate of repeat operations.[1] Surgical resection of tumors in the head and neck can be complicated by proximity to vital structures and could benefit from intraoperative fluorescence molecular imaging strategies.[2,3]

Fluorescence imaging is depth-limited due to signal attenuation from absorption, scattering, and background fluorescence such that even low levels of dye in overlying tissues can obfuscate tumor-specific contrast.[4] Signal attenuation from surface weighting of fluorescence is compounded by even a few percent bleed-through of reflected excitation and ambient light.[5] Eliminating these surface signals is necessary to improve subsurface, cancer-specific fluorescence contrast and better define tumor boundaries. Therefore, we investigated structured illumination techniques for optical sectioning of surface and deep fluorescence signals to aid in oncologic surgery.

Optical sectioning with structured illumination, as demonstrated by Neil et al., uses fluorescence excitation in striped patterns to isolate in-plane versus out-of-plane fluorescence.[6] Thus planar imaged light (I_0) can be deconvolved into spatially modulated (I_S) and constant, unmodulated (I_C) components

$$I_0 = I_S + I_C. \tag{1}$$

When illumination patterns are sequentially phase-shifted by $2\pi/3$, (I_1, I_2, and I_3), I_0 and I_S can be deconvolved according to Eqs. (2) and (3), respectively,

$$I_0 = (I_1 + I_2 + I_3)/3, \tag{2}$$

$$I_S = \frac{\sqrt{2}}{3}\sqrt{(I_1 - I_2)^2 + (I_2 - I_3)^2 + (I_3 - I_1)^2}. \tag{3}$$

The peak-to-trough distance of the excitation pattern is equivalent to fixed source-detector separation of diffuse optical imaging,[7,8] allowing for selective imaging of the desired fluorescence signal.[9] Therefore, the nondepth-dependent signal coming from the tumor (I_C) can be isolated by subtracting the unwanted plane of the shallow signal (I_S) from total fluorescence signal (I_0). In the planar reflectance image (I_0), the unwanted background fluorescence (I_S) obscures the subcutaneous tumor signal (I_C). Extracting the I_C signal from the total I_0 signal elegantly isolates the tumor fluorescence.

Herein we describe structured illumination fluorescent molecular imaging (SIFMI) for enhancing tumor localization in a mouse model of solitary extramedullary plasmacytoma, which most commonly occurs in the head and neck region and expresses high levels of the $\alpha_4\beta_1$ integrin receptor.[10] We compared SIFMI with conventional, uniform illumination planar fluorescence reflectance imaging (PFRI), planar fluorescence imaging normalized by reflectance (normalized),[11] and diffuse optical spectroscopy imaging (DOSI).[12]

Structured illumination techniques such as spatial frequency domain imaging (SFDI) enable rapid measurement of tissue optical properties,[13] mapping hemoglobin oxygenation,[14,15] and assessing tissue perfusion[16] in noncontact, reflection geometry. SFDI methods have produced improved contrast over

1083-3668/2016/$25.00 © 2016 SPIE

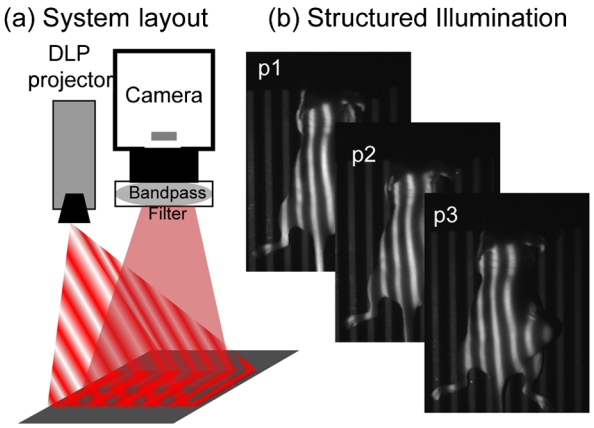

Fig. 1 (a) Design of SIFMI imaging system including DLP projector providing patterned excitation and CMOS camera for fluorescence detection. (b) Excitation patterns (3) projected onto subject for optical sectioning of superficial and deep fluorescence.

conventional planar illumination imaging for improving spatial resolution in phantoms[9] and tissues,[17] quantifying fluorescent reporters in skin[18] and correcting for surface signal attenuation,[17] but this is the first application of structured illumination for subsurface *in vivo* tumor-specific fluorescence contrast enhancement using an near-infrared (NIR) fluorescent tumor-targeted tracer. We demonstrate that SIFMI, in combination with tumor-selective fluorescent molecular probes, enhances contrast to better identify tumors and tumor boundaries *in vivo*, providing full fluorescence information and enabling better clinical decisions by the operator.

Structured illumination patterns were projected by digital micromirror device-based projector (DLP Lightcrafter 4500, Texas Instruments) using only the red light-emitting diode (LED) (624 ± 18 nm) for fluorescence excitation of the fluorescent molecular probe, LLP2A-Cy5 (peak $\lambda ex/\lambda em = 657/676$ nm).[10] An NIR-sensitive complementary metal oxide sensor (CMOS) camera (Firefly MV FMVU-03MTM-CS, Point Grey Research, Canada) captured images after excitation light was blocked by an optical bandpass filter (720 ± 20 nm, 720AF20, Omega Optical, Brattleboro, Vermont). The projector was positioned such that the offset projection uniformly illuminated the imaging platform over the camera field of view [Fig. 1(a)]. Pattern projection and image acquisition were controlled by customized MATLAB® (The Mathworks, Inc., Natick, Massachusetts) code. Premade 8-bit grayscale sinusoidal fringe pattern images, each offset by $2\pi/3$, were projected onto the subject using the red channel of the projector [Fig. 1(b)]. Images were acquired as 16-bit tagged image file format (TIFF) for each illumination pattern, followed by full-field illumination and no illumination (dark) captures. This routine was repeated with a neutral density emission filter in place of the bandpass filter for illumination reference. Initial studies were performed using silicone-based phantoms with optical properties similar to biological tissues and fluorescent inclusions.[19] These studies indicated that fluorescence contrast enhancement was maximized when using a low-frequency sinusoidal pattern of 0.66 cm^{-1}, which was subsequently used for all *in vivo* animal studies.

All animal studies were conducted according to protocols approved by the Washington University Animal Studies Committee. Human multiple myeloma (U266) tumor xenografts were grown by subcutaneous injection of 10^6 cells in the right flank of 8-week-old male NCR-nude mice (Charles River Laboratories, Wilmington, Massachusetts, $n = 2$). When tumors were 1 cm in maximum diameter, mice were anesthetized with isoflurane (2% v/v in 100% O_2) and injected with 2.5-nmol LLP2A-Cy5 in 0.1-mL 4% dimethylsulfoxide in sterile water via the lateral tail vein. LLP2A-Cy5 accumulates in tumors expressing $\alpha_4\beta_1$ integrin and has absorption and emission spectra suitable for our custom developed imaging system.[10] Eighteen hours postinjection, mice were anesthetized and placed prone on the imaging platform of the SIFMI system [Fig. 1(a)]. Image processing and analysis were performed using NIH ImageJ and MATLAB®. Imaging was also performed using the Optix MX3 time-domain DOSI system ($\lambda ex/\lambda em = 670/695$ nm) in a single point source-detector setup with raster scanning (3-mm separation).[8]

Summation of the three phase-shifted fluorescence images using Eq. (2) resulted in I_0 [Fig. 2(a)], which was equivalent to planar fluorescence images acquired with uniform illumination. These I_0 images contained both tumor and background

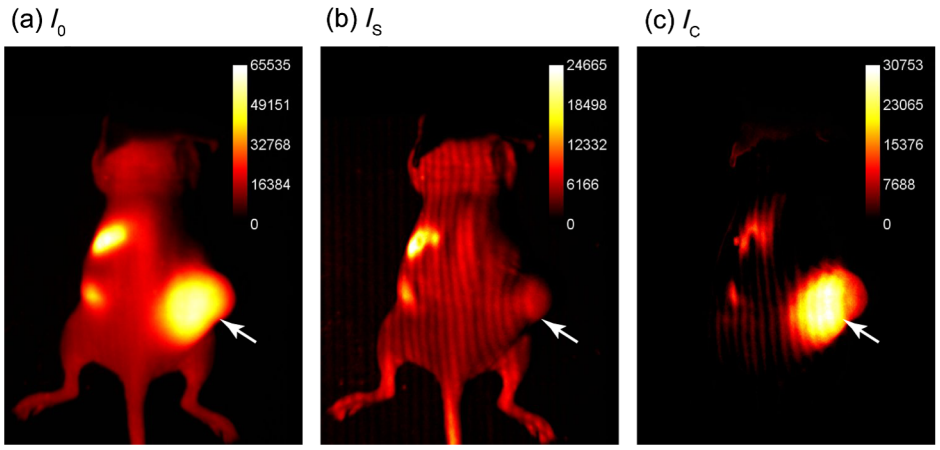

Fig. 2 Demonstration of SIFMI process with subcutaneous tumor xenograft model and NIR fluorescent molecular probe with high affinity for multiple myeloma cancer cells in solid tumor (arrow). (a) Planar fluorescence uniform illumination equivalent image (I_0) reconstructed using the sum of the projected light patterns [Eq. (2)]. (b) Surface signal image (I_S) from the modulated signals [Eq. (3)]. (c) Subsurface, diffuse signal (I_C) according to a modified Eq. (1).

fluorescence, showing high signal throughout the mouse body with the highest signal from the subcutaneous xenograft on the right flank. High signal was also present from the stomach and intestines, presumably from dietary sources. Demodulation of phase-shifted images with frequency-dependent characteristics according to Eq. (3), yielded the surface components in I_S [Fig. 2(b)]. Further image analysis indicated true surface fluorescence signal was equal to twice the values in I_S and subtraction of $2 \times I_S$ improved tumor isolation and reduced background fluorescence, correlating with *ex vivo* fluorescence measurements [Fig. 2(c)].

For comparison of SIFMI to other *in vivo* fluorescence imaging techniques, region-of-interest (ROI) analysis was performed for data acquired using uniform illumination PFRI, fluorescence/reflectance normalization, and DOSI. We first compared the fluorescence intensity spatial distributions obtained using the various methods [Fig. 3(a)]. Conventional PFRI imaging shows peak fluorescence signal intensity from within the tumor with a residual high background fluorescence throughout the mouse body.

Similarly, normalization of the reflectance-geometry fluorescence signal relative to excitation[11] was not effective for enhancing tumor contrast. The DOSI images showed the fluorescence localized to the tumor, with background fluorescence limited to the scattered light traveling to the tissue adjoining the tumor. The SIFMI approach resulted in high signal from the tumor and a striped artifact pattern from incomplete modulated signal subtraction. Comparison of fluorescence intensities from the

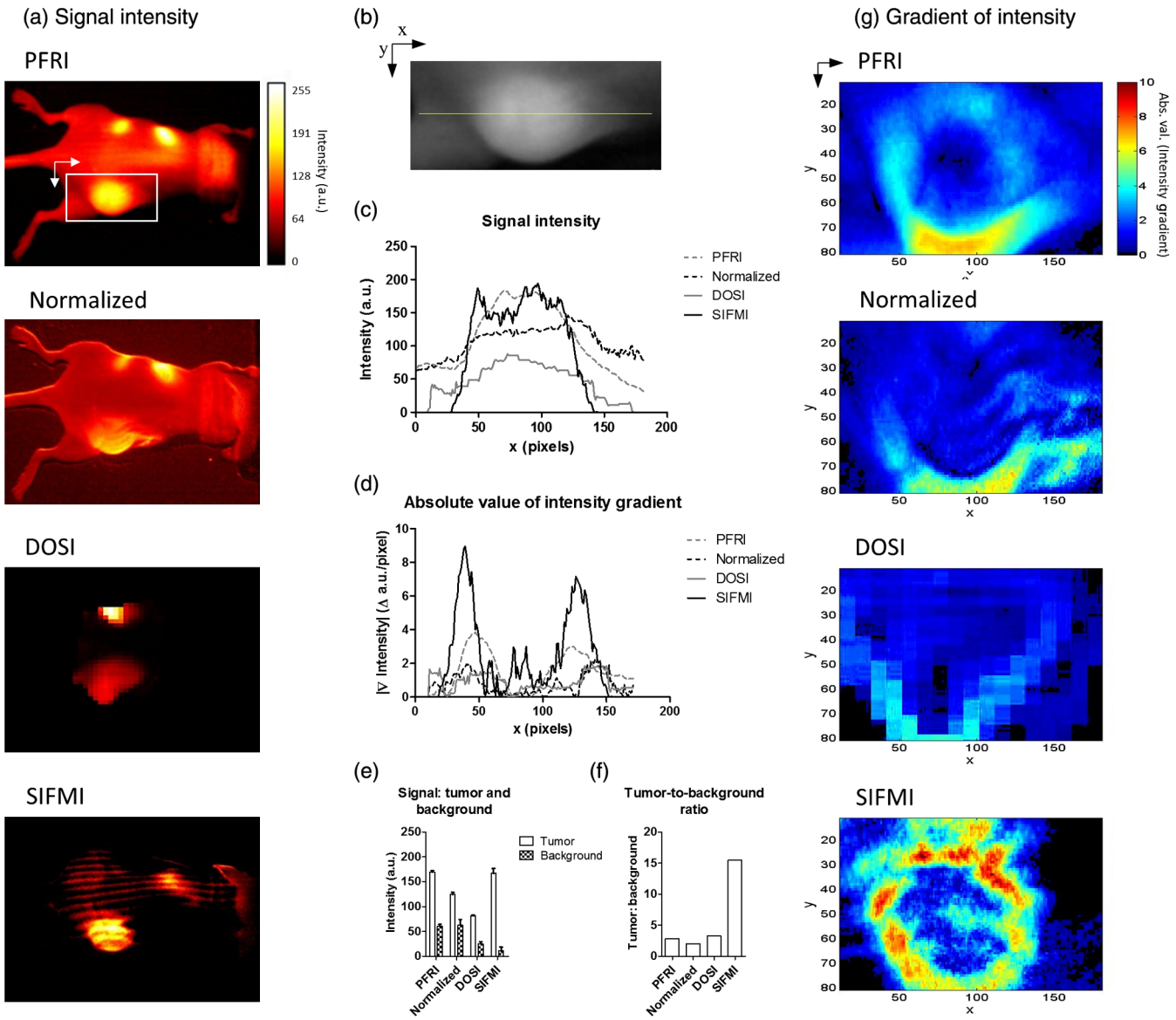

Fig. 3 (a) Fluorescence signal intensity (normalized to 8-bit for visual contrast) for the same mouse imaged using planar imaging, fluorescence/reflectance imaging, diffuse imaging, and structured illumination. (b) Example of ROI analyzed, with yellow line indicating the origin for the values plotted in (c) and (d). (c) Signal intensity plot for each image along yellow line in (b). (d) Absolute value of the gradient of intensity plotted along the line selected. (e) Signal intensity quantified for the tumor region and the non-tumor region. (f) Tumor-to-background ratio calculated using the signal intensity. (g) Absolute value of the gradient of intensity visualized over the ROI for the different imaging methods.

individual images [Fig. 3(c)] using the cross section shown in Fig. 3(b) demonstrated that the SIFMI approach had the highest signal from within the tumor as compared to the signal on either side of the tumor.

ROI analyses of fluorescence intensity values for tumor and nontumor regions followed the initial visual inspection with the PFRI and SIFMI having a high tumor signal [Fig. 3(e)]. SIFMI resulted in higher tumor contrast due to background subtraction, resulting in a fivefold improvement in the tumor-to-background ratio [Fig. 3(f)]. Optimization of projected patterns is needed to remove striping artifacts in the final image.[20] SIFMI corrects for nonspecific surface signals to enhance tumor-specific contrast and can be extended to correct for light attenuation due to heterogeneities in surface colors due to pigmentation or blood.[17]

We further applied spatial gradient mapping to enhance tumor boundary display.[21] The absolute value of the gradient [Fig. 3(d)] was compared for each method via spatial gradient maps, further demonstrating tumor intensity gradient of the SIFMI image was much higher than other methods, providing well-defined boundaries of the tumor [Fig. 3(g)].

The efficient SIFMI technique improves lateral resolution of tumor boundaries by separating in-focus (surface) and out-of-focus (diffusely scattered) signals, enabling rapid fluorescence imaging in wide-field reflection mode with depth sensitivity of DOSI.[22] Further segmentation would require tomographic reconstruction methods.[22–24] The use of striped patterns of different frequencies allows for a clear delineation between the tumor and the background fluorescence. In doing so, tumor contrast enhancement does not rely on arbitrary, user-defined thresholding,[2] and the entirety of the fluorescence information remains visible to the operator, thus preserving detection sensitivity. SIFMI presents a clear cost-benefit advantage and will readily adapt to intraoperative imaging modalities to enhance visualization of fluorescent molecular NIR probes during surgery.

Acknowledgments

This work was supported by grants from the NIH National Cancer Institute: R01CA176221 and the Center for Multiple Myeloma Nanotherapy (U54CA199092). We thank the WU-MDACC Inter-Institutional Molecular Imaging Center (NCI P50CA094056) and the Siteman Cancer Center Small Animal Imaging Core (NCI P30CA091842) for imaging services. The Optix MX3 was purchased by NIH shared instrument Grant No. S10OD016419. The content is solely the responsibility of the authors and does not necessarily represent the official views of the National Institutes of Health.

References

1. L. G. Wilke et al., "Repeat surgery after breast conservation for the treatment of stage 0 to ii breast carcinoma: a report from the national cancer data base, 2004-2010," *JAMA Surg.* **149**(12), 1296–1305 (2014).
2. I. Atallah et al., "Role of near-infrared fluorescence imaging in head and neck cancer surgery: from animal models to humans," *Eur. Arch. Oto-Rhino-Laryngol.* **272**(10), 2593–2600 (2015).
3. B. A. Miles et al., "Operative margin control with high-resolution optical microendoscopy for head and neck squamous cell carcinoma," *Laryngoscope* **125**(10), 2308–2316 (2015).
4. S. Gioux, H. S. Choi, and J. V. Frangioni, "Image-guided surgery using invisible near-infrared light: fundamentals of clinical translation," *Mol. Imaging* **9**(5), 237–255 (2010).
5. B. Zhu et al., "Reduction of excitation light leakage to improve near-infrared fluorescence imaging for tissue surface and deep tissue imaging," *Med. Phys.* **37**(11), 5961–5970 (2010).
6. M. A. Neil, R. Juskaitis, and T. Wilson, "Method of obtaining optical sectioning by using structured light in a conventional microscope," *Opt. Lett.* **22**(24), 1905–1907 (1997).
7. D. Maji et al., "Noninvasive imaging of focal atherosclerotic lesions using fluorescence molecular tomography," *J. Biomed. Opt.* **19**(11), 110501 (2014).
8. M. Solomon et al., "Detection of enzyme activity in orthotopic murine breast cancer by fluorescence lifetime imaging using a fluorescence resonance energy transfer-based molecular probe," *J. Biomed. Opt.* **16**(6), 066019 (2011).
9. A. Mazhar et al., "Structured illumination enhances resolution and contrast in thick tissue fluorescence imaging," *J. Biomed. Opt.* **15**(1), 010506 (2010).
10. D. Soodgupta et al., "Ex vivo and in vivo evaluation of over-expressed VLA-4 in multiple myeloma using LLP2A imaging agents," *J. Nucl. Med.* (2016).
11. K. Calabro et al., "Gender variations in the optical properties of skin in murine animal models," *J. Biomed. Opt.* **16**(1), 011008 (2011).
12. V. Ntziachristos et al., "Planar fluorescence imaging using normalized data," *J. Biomed. Opt.* **10**(6), 064007 (2005).
13. D. J. Cuccia et al., "Quantitation and mapping of tissue optical properties using modulated imaging," *J. Biomed. Opt.* **14**(2), 024012 (2009).
14. S. Gioux et al., "First-in-human pilot study of a spatial frequency domain oxygenation imaging system," *J. Biomed. Opt.* **16**(8), 086015 (2011).
15. A. Mazhar et al., "Wavelength optimization for rapid chromophore mapping using spatial frequency domain imaging," *J. Biomed. Opt.* **15**(6), 061716 (2010).
16. J. T. Nguyen et al., "A novel pilot study using spatial frequency domain imaging to assess oxygenation of perforator flaps during reconstructive breast surgery," *Ann. Plast. Surg.* **71**(3), 308–315 (2013).
17. B. Yang, M. Sharma, and J. W. Tunnell, "Attenuation-corrected fluorescence extraction for image-guided surgery in spatial frequency domain," *J. Biomed. Opt.* **18**(8), 080503 (2013).
18. R. B. Saager et al., "Quantitative fluorescence imaging of protoporphyrin IX through determination of tissue optical properties in the spatial frequency domain," *J. Biomed. Opt.* **16**(12), 126013 (2011).
19. S. Keren et al., "A comparison between a time domain and continuous wave small animal optical imaging system," *IEEE Trans. Med. Imaging* **27**(1), 58–63 (2008).
20. A. J. Lin et al., "Visible spatial frequency domain imaging with a digital light microprojector," *J. Biomed. Opt.* **18**(9), 096007 (2013).
21. J. P. Miller et al., "Gradient-based algorithm for determining tumor volumes in small animals using planar fluorescence imaging platform," *Tomography* **2**(1), 17–25 (2016).
22. S. Belanger et al., "Real-time diffuse optical tomography based on structured illumination," *J. Biomed. Opt.* **15**(1), 016006 (2010).
23. J. Angelo et al., "Depth-enhanced fluorescence imaging using masked detection of structured illumination," *J. Biomed. Opt.* **19**(11), 116008 (2014).
24. T. D. O'sullivan et al., "Diffuse optical imaging using spatially and temporally modulated light," *J. Biomed. Opt.* **17**(7), 071311 (2012).